Theor Chem Acc (2009) 124:355–363
DOI 10.1007/s00214-009-0620-2

REGULAR ARTICLE

Reaction force analyses of nitro-*aci* tautomerizations of trinitromethane, the elusive trinitromethanol, picric acid and 2,4-dinitro-1H-imidazole

Jane S. Murray · Pat Lane · Michael Göbel · Thomas M. Klapötke · Peter Politzer

Received: 27 June 2009 / Accepted: 28 July 2009 / Published online: 19 August 2009

Abstract We have analyzed computationally, in terms of the reaction force, the nitro → *aci* tautomerizations of trinitromethane, trinitromethanol, picric acid and 2,4-dinitro-1H-imidazole. These processes involve intramolecular transfer of a hydrogen to an NO_2 oxygen, forming the *aci* tautomer (a nitronic acid). The reaction force naturally and unambiguously divides an activation barrier into two components: (1) the energy required for initial structural changes in the reactant(s), and (2) the energy associated with the first portion of the transition to product(s). In each of these tautomerizations, the first component is dominant. For trinitromethane, it is so large that the resulting total activation barrier makes C–NO_2 bond scission energetically preferable. On the other hand, trinitromethanol—which appears to be unknown—readily undergoes fragmentation in conjunction with hydrogen transfer. Picric acid has the interesting feature that the reaction is almost complete after the first portion of the activation process, marked by the minimum of the reaction force. In all four reactions, the properties of the systems at the force minimum, transition state and force maximum are consistent with the concept of a "transition" region in a chemical reaction versus simply a transition state.

Keywords Nitro-*aci* tautomerization · Reaction force analysis · Trinitromethane · Trinitromethanol · Picric acid · 2,4-dinitro-1H-imidazole

J. S. Murray (✉) · P. Lane · P. Politzer
Department of Chemistry, University of New Orleans, New Orleans, LA 70148, USA
e-mail: jsmurray@uno.edu

J. S. Murray · P. Politzer
Department of Chemistry, Cleveland State University, Cleveland, OH 44115, USA

M. Göbel · T. M. Klapötke
Department of Chemistry and Biochemistry, University of Munich, Butenandtstr. 5-13 (D), 81377 Munich, Germany

T. M. Klapötke
CECD, Departments of Mechanical Engineering and Chemistry/Biochemistry, University of Maryland, College Park, MD 20742, USA

1 Nitro-*aci* tautomerization

It is well known that some nitro derivatives containing the C–NO_2 linkage can undergo intramolecular transfer of a hydrogen to one of the nitro oxygens, forming an *aci* tautomer **1** [1–3].

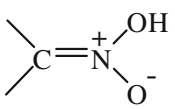

1

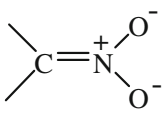

2

These *aci* tautomers are called nitronic acids; their pK_a values are usually between 2 and 6. They are quite reactive, and are important intermediates in organic synthesis, e.g. the Nef reaction. However, they are often rather uns€, with half-lives measured in hours and days.

In the area of energetic materials, *aci* tautomerization is of particular importance because it is a possible early step in decomposition processes that are involved in detonation [4–6]. For example, in developing their oxygen balance correlations for the impact sensitivities of energetic compounds, Kamlet and Adolph found it necessary to treat separately the nitroaromatics with a C–H on an alkyl group

ortho to an NO_2 [7]. Such compounds may be decomposing via *aci* tautomerization. The nitronate anion, **2**, has also been implicated in decompositions [8, 9].

We have recently carried out a preliminary computational investigation of the gas phase *aci* tautomerization of trinitromethane (**3**, nitroform) [10]. This is a well-known compound, which has been characterized crystallographically [11] and has applications in synthesis and in propellant formulations [12]. With the three strongly electron-withdrawing NO_2 groups, it might be anticipated that proton transfer to one of the oxygens would be rather facile. Indeed, Schödel et al. described the *aci* tautomer of **3** as a "tempting target" [11]. To our knowledge, however, it has not been isolated, although there are reports that it may have been obtained but is quite unstable [2, 13–15]. We found the activation barrier to *aci* tautomerization to be 45 kcal/mol at the B3PW91/6-31++G(3d,2p) level, which could be viewed as surprisingly high given the expected acidity of the hydrogen.

Trinitromethanol (**4**) is structurally closely related to **3**, a hydroxyl group replacing the hydrogen. It should also be a prime candidate for *aci* tautomerization, since its hydrogen would be anticipated to be even more acidic than that of **3**. As far as we are aware, however, neither **4** nor *aci*-**4** is known.

To better understand what is occurring (or not occurring) in these systems, we undertook a detailed computational study of the proposed gas phase *aci* tautomerizations of **3** and **4**. We also included two well-established energetic compounds, picric acid (**5**) and 2,4-dinitro-1H-imidazole (**6**) [16]. Since a competing decomposition route is always the rupture of a C–NO_2 bond, we have also determined the energy and enthalpy that this would require in each case. The analysis of the tautomerizations was carried out in terms of the reaction force, which we shall now briefly discuss.

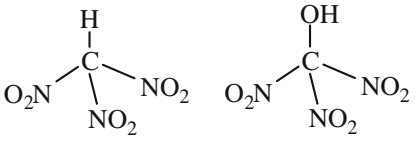

3

4

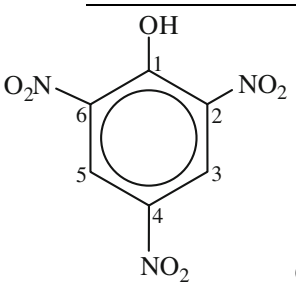

5

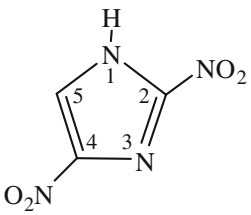

6

2 The reaction force

The progress of a chemical process can be followed by the change in the potential energy V(**R**) of the system along an appropriate reaction coordinate **R**. The profile of V(**R**), such as that in Fig. 1a for a one-step process A → B, indicates the relative energies of the reactants, transition state and products. However, V(**R**) contains much more information, some of which can be extracted by taking its negative gradient along **R**, yielding the classically-defined reaction force **F**(**R**), Fig. 1b.

$$\mathbf{F}(\mathbf{R}) = -\frac{\partial V(\mathbf{R})}{\partial \mathbf{R}} \tag{1}$$

R is normally taken to be the intrinsic reaction coordinate, i.e. the minimum-energy path, in mass-weighted coordinates, that links the transition state to the reactants and products [17, 18].

F(**R**) has a minimum at α and a maximum at γ, the inflection points of V(**R**). These partition the reaction, in a natural and non-arbitrary manner, into three regions: the first is the one prior to the **F**(**R**) minimum, A → α; the second is between the **F**(**R**) minimum and maximum, $\alpha \rightarrow \gamma$; and the third is after the **F**(**R**) maximum, γ → B.

The general characteristics of these regions have been examined in a series of studies [19–39] which include, S_N2 substitution (gas phase and in solution) [25, 28, 33], Markovnikov and anti-Markovnikov addition to a double bond (gas phase and in solution) [39], cycloaddition to olefins [37], bond dissociation [27, 35, 36], single and double proton transfer [20–24, 26] (in one instance involving two potential barriers [30]), and structural isomerization [20]. It was found that the first region, A → α, is usually dominated by structural changes within the reactants, e.g. bond stretching, rotations, angle-bending, etc. **F**(**R**) reflects the resistance to these changes, and is increasingly retarding (i.e. negative), reaching its extremum at α; at this point, the system can be viewed roughly as distorted states of the reactants. In the second region, $\alpha \rightarrow \gamma$, occurs the major portion of the transition to products: bonds break, new ones form, there may be rapid and extensive changes in properties, such as electrostatic potentials and ionization energies. All of this is manifested in a growing driving force, which causes **F**(**R**) to increase steadily until it reaches a maximum at γ. At the beginning of the third region, which is γ → B, the system can

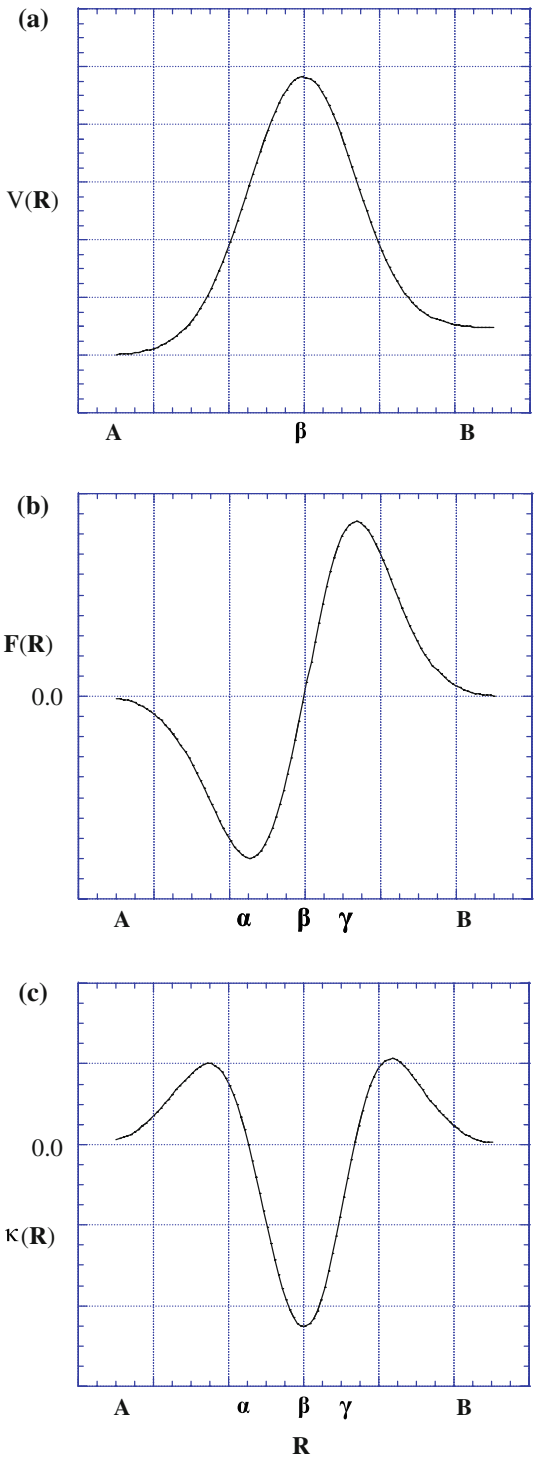

Fig. 1 Typical profiles of **a** the potential energy V(**R**), **b** the reaction force **F**(**R**) and **c** the position-dependent reaction force constant κ(**R**) along the intrinsic reaction coordinate **R**. The points R = α and R = γ correspond to the minimum and the maximum of **F**(**R**); the transition state is at R = β. The zeroes of **F**(**R**) and κ(**R**) are indicated

often be regarded as distorted versions of the products, which gradually relax to their final states. In view of these overall characteristics of the three regions, they are commonly designated as the reactant (A → α), transition (α → γ) and product (γ → B) regions.

An important feature of reaction force analysis is that it shows the activation energy to be the sum of two components—the energies needed to go (a) from the reactants to the force minimum at α, and (b) from α to the transition state at β:

$$\begin{aligned}\Delta E_{act} &= V(\beta) - V(A) = [V(\beta) - V(\alpha)] + [V(\alpha) - V(A)] \\ &= \Delta E_{act,2} + \Delta E_{act,1} \end{aligned} \quad (2)$$

$\Delta E_{act,1}$ is largely the energy required to overcome the system's resistance to the structural changes in the reactant region between A and α, while $\Delta E_{act,2}$ supports the first portion of the transition to products, α → β. It has been demonstrated that this division of ΔE_{act} into its two parts helps to explain how external agents, such as solvents and catalysts, affect reaction rates, i.e. whether they change mainly the structural or the electronic component of ΔE_{act} or both [26, 28, 39]. For example, in the S_N2 substitution $H_2O + CH_3Cl \rightarrow HCl + CH_3OH$, the effect of aqueous solution was found to be not upon the transition state but rather in facilitating the initial stretching of the C–Cl bond [28]. In the keto-enol tautomerization of thymine, the presence of Mg(II) as a catalyst also affects the first (reactant) portion of the activation process (prior to the force minimum) [26]. However, in the addition of HCl to $H_3C–CH=CH_2$, chloroform solvent influences primarily the second part of the activation, α → β, approaching the transition state [39].

Finally, an additional insight into reaction mechanisms is obtained from the second derivative of V(**R**), the reaction force constant κ(**R**):

$$\kappa(\mathbf{R}) = \frac{\partial^2 V(\mathbf{R})}{\partial \mathbf{R}^2} = -\frac{\partial \mathbf{F}(\mathbf{R})}{\partial \mathbf{R}} \quad (3)$$

For the V(**R**) and **F**(**R**) in Fig. 1a and b, κ(**R**) has the form shown in Fig. 1c; note that it is negative throughout the entire transition region between α and γ [34, 37].

The transition state of a reaction is commonly identified by the presence of a negative force constant for one normal vibrational mode. However, the work of Zewail and Polanyi in transition state spectroscopy has led to the concept of a reaction having a continuum of transient, unstable configurations, a transition region rather than a single transition state [40, 41]. The reaction force constant κ(**R**) reflects this continuum, and shows it to be bounded by the minimum and the maximum of **F**(**R**), at which κ(**R**) = 0.

3 Procedures and results

The geometries and energies of **3**–**6** along the intrinsic reaction coordinates for their conversions from the nitro to the *aci* tautomers, which involves a large number of points,

were computed with the B3PW91/6-31+G(d,p) procedure. The C–NO_2 bond dissociation energies and enthalpies of **3–6** at 298 K were calculated with a larger basis set, B3PW91/6-31++G(3d,2p), to be consistent with those obtained earlier for other NO_2-containing molecules [10, 42]. Using the two different basis sets does not preclude comparing the 6-31+G(d,p) activation energies with the 6-31++G(3d,2p) dissociation energies, as we will do later, because we confirmed, using **3** and **4** as test cases, that the ΔE_{act} (298 K) computed with the two different basis sets are within 0.3 kcal/mol of each other.

The geometries and relative energies of **3–6** at the five key points A, α, β, γ and B are in Tables 1, 2, 3, 4, which also depict each of these structures graphically. The activation energies and their components $\Delta E_{act,1}$ and $\Delta E_{act,2}$ are summarized in Table 5. The C–NO_2 bond dissociation energies and enthalpies are listed in Table 6.

4 Discussion

4.1 Trinitromethane

The structure of the ground-state of trinitromethane (**3**, Table 1) shows that the NO_2 groups have a propeller-like arrangement; the H–C–N–O dihedral angles are 139° and −42°. The oxygens are in two distinct planes, one from each NO_2 group being closer to the hydrogen and the other farther from it. This is typical of trinitromethyl derivatives [10, 43–47], and has been explained in terms of intramolecular N···O electrostatic interactions involving the oxygens farther from the hydrogen [10, 46, 47].

Table 1 shows the structural changes that would accompany hydrogen migration to one of the closer oxygens, Eq. 4. The propeller-like structure is quickly disrupted.

(4)

At α, the **F**(**R**) minimum, NO_aO_b (the nitro group toward which the hydrogen is moving) is coplanar with the stretched C–H bond and the other two NO_2 groups are approximately perpendicular to it.

These relative orientations remain throughout the transition region, between the **F**(**R**) minimum at α and its maximum at γ. The stretched C–H bond breaks and a stretched O_a–H bond forms. A striking feature is that the carbon retains a quasi-tetrahedral configuration and the C–NO_aO_b bond length remains essentially unchanged from the reactant all the way through the transition region, to γ. However, the system is rather unstable at γ, 28 kcal/mol above the final product (Table 1). The carbon now changes rapidly to a trigonal configuration with a C=N(O_b)O_aH double bond, while one of the other two NO_2 groups rotates by about 90° in going to the *aci* product.

Table 1 Computed structures, relative energies at 298 K and some distance/angle data at points along intrinsic reaction coordinate for conversion of trinitromethane, **3**, to its *aci* tautomer, Eq. 4

	Reactant	Force min, α	Transition state, β	Force max, γ	Product
	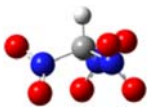	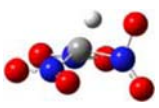	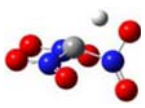	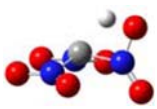	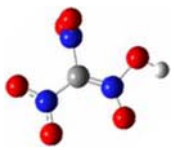
Relative E (298 K)	0.0	28.8	45.2	41.6	13.4
Bond lengths					
C–H	1.087	1.179	1.485	1.768	3.017
C–NO_aO_b	1.515	1.515	1.517	1.510	1.318
N–O_a	1.216	1.270	1.295	1.316	1.390
N–O_b	1.212	1.189	1.179	1.178	1.218
O_a–H	2.480	1.565	1.199	1.019	0.976
Angles					
N–C–H	109	80	67	63	22
C–N–O_a–H	−19	0	0	0	178

The hydrogen moves to oxygen O_a of a neighboring NO_2. Energies are in kcal/mol, distances in Angstroms and angles in degrees
Colors of atoms: carbon is gray, hydrogen is white, nitrogens are blue and oxygens are red

Table 2 Computed structures, relative energies at 298 K and some distance/angle data at points along intrinsic reaction coordinate for conversion of trinitromethanol, **4**, to its *aci* tautomer, Eq. 5

	Reactant	Force min, α	Transition state, β	Force max, γ	Product complex
	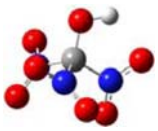	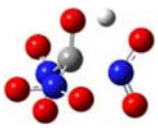	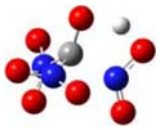	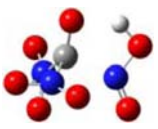	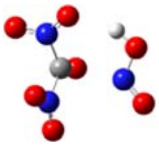
Relative E (298 K)	0.0	6.2	9.5[a]	9.8[a]	0.8
Bond lengths					
C–O	1.319	1.276	1.243	1.221	1.173
O–H	0.982	1.086	1.356	1.559	3.739
C–NO_aO_b	1.555	1.712	1.736	1.796	2.914
N–O_a	1.222	1.250	1.279	1.302	1.380
N–O_b	1.204	1.190	1.180	1.175	1.180
O_a–H	1.922	1.373	1.117	1.030	0.976
Angle					
O_a–N–C–O	15	2	2	2	98

The hydrogen moves to oxygen O_a of a neighboring NO_2. Energies are in kcal/mol, distances in Angstroms and angles in degrees

Colors of atoms: carbon is gray, hydrogen is white, nitrogens are blue and oxygens are red

[a] The energy at 0 K at the transition state, β, is 0.8 kcal/mol higher than that at the **F**(**R**) maximum, γ. However, inclusion of zero-point energies and thermal corrections to 298 K puts E(γ) above E(β) by 0.3 kcal/mol

Why does the process just described have a computed activation barrier as high as 45 kcal/mol (Table 5), given the acidic nature of the hydrogen in trinitromethane due to the three NO_2 groups [48]? To answer this, note the first component of the activation energy, $\Delta E_{act,1} = 29$ kcal/mol. This amount of energy is required just for the structural changes in the reactant region, prior to the **F**(**R**) minimum. It is needed to partially disrupt the ground-state N···O interactions in the propeller-like arrangement of the NO_2 groups and also for the concomitant stretching of the C–H bond, which must overcome significant H···O attractions between the hydrogen and the three closer oxygens [10].

However, the relatively high activation barrier, and specifically $\Delta E_{act,1}$, is only part of the explanation for the challenge posed by the "tempting target," *aci*-trinitromethane [11]. In general, the introduction of additional NO_2 groups tends to weaken existing C–NO_2 bonds, particularly on the same carbon [42]. Thus, the C–NO_2 bond energy in H_3C–NO_2 is about 60 kcal/mol [49], but it is only 37 kcal/mol in $HC(NO_2)_3$, **3** (Table 6). Since this is less than the activation energy for going to *aci*-**3**, 45 kcal/mol, it is likely that C–NO_2 bond rupture occurs preferentially.

4.2 Trinitromethanol

The NO_2 groups in ground-state trinitromethanol, **4**, are not in the propeller-like arrangement observed in **3**. In **4**, one of them, NO_aO_b, is nearly coplanar with the C–O–H portion of the molecule, while the other two are approximately perpendicular to each other (Table 2). This permits O–H···O_a hydrogen bonding; the H···O_a separation is 1.922 Å, while the sum of the van der Waals radii is 2.72 Å [50]. It is to O_a that the hydrogen will migrate. However, our calculations indicate that in the gas phase the result will not be an *aci* tautomer. Instead, **4** breaks up into a weakly-bound complex of $(O_2N)_2C{=}O$ and HO_aNO_b, Eq. 5, which is lower in energy by only 0.4 kcal/mol relative to the separate molecules.

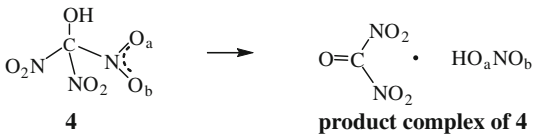

4 **product complex of 4** (5)

It is apparent already by the **F**(**R**) minimum at α that the course of Eq. 5 will be different from the process for **3** given in Eq. 4. In contrast to **3** and the other molecules to be discussed (**5** and **6**), the C–NO_aO_b bond in **4** begins to *lengthen* as the hydrogen moves toward O_a, and by the **F**(**R**) minimum, it has increased from 1.555 to 1.712 Å. Thus there is already an indication of the forthcoming separation into two molecules. This fragmentation has a very low activation barrier, 10 kcal/mol (Table 5), so it is not surprising that **4** is, we believe, not known. Note that this barrier is less than the dissociation energy of the

Table 3 Computed structures, relative energies at 298 K and some distance/angle data at points along intrinsic reaction coordinate for conversion of picric acid, **5**, to its *aci* tautomer, Eq. 6

	Reactant	Force min, α	Transition state, β	Force max, γ	Product
		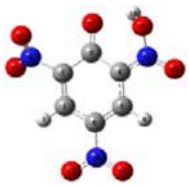	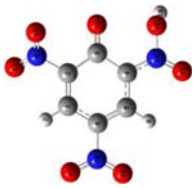		
Relative E (298 K)	0.0	23.3	31.0	29.0	26.2
Bond lengths					
C_1–O	1.313	1.232	1.221	1.219	1.220
O–H	0.993	1.951	2.668	3.126	3.518
C_1–C_2	1.423	1.483	1.494	1.497	1.492
C_2–C_3	1.391	1.415	1.421	1.421	1.421
C_3–C_4	1.382	1.364	1.361	1.362	1.361
C_4–C_5	1.394	1.424	1.429	1.429	1.428
C_5–C_6	1.380	1.358	1.354	1.353	1.353
C_6–C_1	1.417	1.467	1.475	1.476	1.477
C_2–NO_aO_b	1.453	1.366	1.353	1.353	1.356
N–O_a	1.246	1.373	1.380	1.369	1.356
N–O_b	1.215	1.211	1.216	1.220	1.225
O_a–H	1.645	0.988	0.974	0.974	0.977
Angles					
O–O_a–H	13	37	81	113	167
C_2–N–O_a–H	0	55	106	138	179

Numbering of atoms is shown in Eq. 6. The hydroxyl hydrogen moves to oxygen O_a of neighboring NO_2 on C_2. Energies are in kcal/mol, distances in Angstroms and angles in degrees

Colors of atoms: carbons are gray, hydrogens are white, nitrogens are blue and oxygens are red

$C–NO_aO_b$ bond alone, 30 kcal/mol (which is the lowest in Table 6), because Eq. 5 also produces a new bond, O_a–H, and converts the C–O into a double bond.

As the hydrogen migrates toward O_a, it continues to have some attractive interaction with the oxygen that it left. After the **F**(**R**) maximum at γ, however, the $(O_2N)_2C=O$ and $H–O_a–N–O_b$ portions of the system rotate relative to each other, and the weak product complex appears to be stabilized mainly by the hydrogen interacting with an NO_2 oxygen of $(O_2N)_2C=O$; this O···H distance is 2.04 Å, considerably less than the 2.72 Å sum of the van der Waals radii [50].

4.3 Picric acid

Nitro-*aci* tautomerization has frequently been invoked as a possible step in the decomposition and detonation of picric acid, **5** [5, 6]. The process, Eq. 6, has some interesting and unusual features (Table 3). In gas phase picric acid, there is a very strong hydrogen bond between the hydroxyl hydrogen and oxygen O_a of the *ortho* NO_2 group on C_2. The H···O_a separation is only 1.645 Å, just slightly more than the van der Waals radius of oxygen alone, 1.52 Å [50]. The strength of this OH···O_a interaction can be seen by noting that the ΔE (298 K) for the removal of the NO_aO_b group is 9 kcal/mol greater than that for the other *ortho* NO_2 (Table 6).

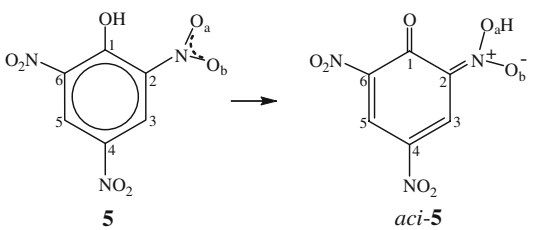

(6)

The strong OH···O_a hydrogen bond and very short H···O_a distance can be interpreted as indicating that the hydrogen migration is already significantly underway in the ground-state of picric acid. The remarkable consequence, as can be seen from the structural data in Table 3, is that the tautomerization process is largely complete already at the **F**(**R**) minimum! All that remains is a rotation

Table 4 Computed structures, relative energies at 298 K and some distance/angle data at points along intrinsic reaction coordinate for conversion of 2,4-dinitro-1H-imidazole, **6**, to its *aci* tautomer, Eq. 7

	Reactant	Force min, α	Transition state, β	Force max, γ	Product
	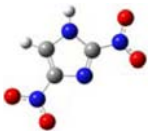				
Relative E (298 K)	0.0	13.8	20.0	19.1	16.4
Bond lengths					
N_1–H	1.013	1.086	1.307	1.447	1.904
N_1–C_2	1.364	1.351	1.355	1.357	1.367
C_2–N_3	1.305	1.313	1.321	1.327	1.346
N_3–C_4	1.351	1.345	1.339	1.336	1.318
C_4–C_5	1.384	1.410	1.415	1.418	1.434
C_5–N_1	1.356	1.346	1.337	1.329	1.322
C_2–NO_aO_b	1.444	1.418	1.405	1.396	1.368
N–O_a	1.234	1.278	1.304	1.318	1.360
N–O_b	1.215	1.204	1.200	1.199	1.199
O_a–H	2.408	1.536	1.231	1.095	0.993
Angles					
C_2–N_1–H	125	102	92	88	82
H–O_a–N–C_2	0	0	0	0	0

Numbering of atoms is shown in Eq. 7. The hydrogen on N_1 moves to oxygen O_a of the neighboring NO_2 on C_2. Energies are in kcal/mol, distances in Angstroms and angles in degrees

Colors of atoms: carbons are gray, hydrogens are white, nitrogens are blue and oxygens are red

Table 5 Computed activation energies ΔE_{act} and their components $\Delta E_{act,1}$ and $\Delta E_{act,2}$ for the four *aci* tautomerizations, Eqs. 4–7, at 298 K

Molecule	Reaction	$\Delta E_{act,1}$	$\Delta E_{act,2}$	ΔE_{act}
Trinitromethane, **3**	Eq. 4	28.8	16.4	45.2
Trinitromethanol, **4**	Eq. 5	6.2	3.4	9.5
Picric acid, **5**	Eq. 6	23.3	7.7	31.0
2,4-Dinitro-1H-imidazole, **6**	Eq. 7	13.8	6.2	20.0

Values are in kcal/mol; Computational level: B3PW91/6-31+G(d,p)

Table 6 Computed C–NO_2 bond dissociation energies and enthalpies at 298 K for molecules **3**–**6**

Molecule	Bond	ΔE	ΔH
Trinitromethane, **3**	C–NO_2	36.9[a]	37.5[a]
Trinitromethanol, **4**	C–NO_2[b]	29.8	30.4
Picric acid, **5**	C_2–NO_2	68.6	69.2
	C_4–NO_2	66.0	66.5
	C_6–NO_2	59.6	60.2
2,4-Dinitro-1H-imidazole, **6**	C_2–NO_2	67.2[c]	67.8[c]
	C_4–NO_2	67.9[c]	68.5[c]

Numbering of atoms in **5** and **6** is given in Eqs. 6 and 7. Values are in kcal/mol, Computational level: B3PW91/6-31++G(3d,2p)

[a] Ref. [10]

[b] ΔE and ΔH have essentially the same values for all three bonds, because dissociation of each C–NO_2 leads to the same radicals, $(O_2N)_2C$–OH and NO_2

[c] Ref. [42]

of the hydrogen. The new H–O_a bond gradually moves through 180° until the hydrogen is quite near (2.13 Å) to the other NO_2 oxygen, O_b; note the changes in the C_2–N–O_a–H dihedral angle. All of the other internuclear distances listed in Table 3 are, to a striking degree, virtually unchanged after the **F**(**R**) minimum at α, by which point the molecular framework has already acquired the quinoid structure of the product *aci*-**5**, Eq. 6. This unusual situation of a reaction taking place almost entirely before the **F**(**R**) minimum is reflected in $\Delta E_{act,1}$ being 3 times as large as $\Delta E_{act,2}$ (Table 5). The 8 kcal/mol that comprises $\Delta E_{act,2}$ is needed primarily to overcome the remaining interaction between the hydrogen and the hydroxyl oxygen, which are still within about 1.95 Å of each other. After the transition state at β, the energy of the system changes very little, the small decrease reflecting the H···O_b interaction.

The *aci* tautomerization of **5** requires much less energy than does C–NO_2 bond-breaking (31 kcal/mol, Table 5 vs. 60–69 kcal/mol, Table 6), and accordingly is a more likely decomposition route. Indeed, Brill and James concluded, on the basis of experimental studies, that the initial decomposition step of picric acid involves the tautomer *aci*-**5** [5]. However, reversion to the nitro tautomer has only a small barrier, 5 kcal/mol (Table 3).

4.4 2,4-Dinitro-1H-imidazole

In Table 4 the computed data pertaining to the *aci* tautomerization of 2,4-dinitro-1H-imidazole, **6**, are given.

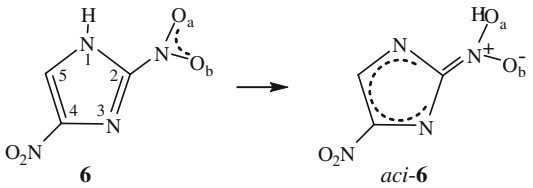

(7)

in which the hydrogen on N_1 moves to O_a on the neighboring NO_2 group, Eq. 7. The main event in the reactant region, prior to the **F**(**R**) minimum at α, is that the angle C_2–N_1–H decreases by 23°, from 125° to 102°. This, coupled with the stretching of the N_1–H bond from 1.013 Å to 1.086 Å, brings the hydrogen to within 1.536 Å of O_a, compared to the original separation of 2.408 Å. The energy required for these structural changes largely accounts for $\Delta E_{act,1}$ being 2/3 of the total activation energy (Table 5); the result is to put the hydrogen well on its way to the target oxygen.

The transition region between α and γ sees the breaking of the N_1–H bond and the formation of the O_a–H. In the product region, the O_a–H bond relaxes from its stretched length of 1.095 Å at the **F**(**R**) maximum, γ, to its final 0.993 Å. Throughout its migration, the hydrogen remains in the plane of the NO_2 group; the H–O_a–N–C_2 dihedral angle is zero along the intrinsic reaction coordinate (Table 4).

The activation energy for this reaction is 20 kcal/mol. Since the C–NO_2 bond dissociation energies of **6** are 67–68 kcal/mol (Table 6), *aci* tautomerization is clearly favored over C–NO_2 rupture as a decomposition pathway. However, the activation energy for the reverse of Eq. 7 is predicted to be only 4 kcal/mol in the gas phase (Table 4), meaning that the *aci* tautomer can readily revert to the nitro form **6**, similarly to what was found for the reverse process of Eq. 6.

5 Summary

The four *aci* tautomerizations that have been discussed show some striking differences. The activation barriers cover a wide range, from 10 to 45 kcal/mol (Table 5). Two of these processes may not even occur; for trinitromethane, **3**, the barrier is so high (45 kcal/mol) that C–NO_2 bond scission is energetically preferable, while for trinitromethanol, **4**, the potential tautomerization leads to quite facile fragmentation, $\Delta E_{act}(298\ K) < 10$ kcal/mol. Picric acid, **5**, and 2,4-dinitro-1H-imidazole, **6**, have intermediate activation energies and *aci* tautomerization is feasible, although the nitro $\leftrightarrow$ *aci* equilibria favor the nitro forms.

However, the reaction force analyses bring out some basic similarities between the four processes. The major structural changes (apart from the continuing movement of the hydrogen) are usually in the reactant and the product regions, before the **F**(**R**) minimum at α and after its maximum at γ. Correspondingly, the largest energy increments are associated with the reactant and product regions (Tables 1, 2, 3, 4). Thus, the first component of the activation energy, $\Delta E_{act,1}(A \rightarrow \alpha)$, is in each instance larger than the second, $\Delta E_{act,2}(\alpha \rightarrow \beta)$. (The same is true for the reverse reactions, for which the present product region becomes the reactant region, with opposite signs for the energy increments, and the **F**(**R**) minimum is at γ.)

In the transition regions of these reactions, the structural changes tend to be more gradual and the energy increments smaller. This is illustrated by the structures shown in Tables 1, 2, 3, 4, corresponding to the positions of the force minima, transition states and force maxima. (Picric acid is an extreme example in that, except for the rotation of the hydrogen around O_a, the reaction is nearly complete already at the **F**(**R**) minimum α.) These features of the transition regions are fully consistent with the Polanyi-Zewail concept of a continuum of transient, unstable configurations [40, 41], which in turn reflects the negative character of the reaction force constant κ(**R**) in the transition region, between the minimum and the maximum of the reaction force **F**(**R**).

Our discussion has focused upon the reactions in Eqs. 4–7 in the gas phase. Other environments, e.g. solution or crystalline, might significantly affect the kinetics and/or mechanisms. As was shown earlier [26, 28, 39] reaction force analysis can be used as well to assess the effects of such external factors.

Acknowledgments JSM, PL and PP appreciate the support of the Defense Threat Reduction Agency, Contract No. HDTRA1-07-1-0002, Project Office Dr. William Wilson, and MG and TMK support of the European Research Office (ERO) of the U.S. Army Research Laboratory (ARL) and Armament Research, Development and Engineering Center (ARDEC) as well as the Strategic Environmental Research and Development Program (SERDP) under contract nos. W911NF-09-2-0018 (ARL), W911NF-09-1-0120 (ARDEC), W011NF-09-1-0056 (ARDEC) and 10 WPSEED01-002/WP-1765 (SERDP).

References

1. Morrison H, Migdalof BH (1965) J Org Chem 30:3996
2. Nielsen AT (1969) In: Feuer H (ed) The chemistry of the nitro and nitroso groups, Part 1, chap 7. Wiley-Interscience, New York
3. Patai S (ed) (1982) The chemistry of amine, nitroso and nitro compounds and their derivatives. Wiley, New York
4. McKee ML (1986) J Am Chem Soc 108:5784–5792
5. Brill TB, James KJ (1993) Chem Rev 93:2667–2692
6. Bharatam PV, Lammertsma K (2003) In: Politzer P, Murray JS (eds) Energetic materials. Part 1. Decomposition, crystal and molecular properties, chap 3. Elsevier, Amsterdam
7. Kamlet MJ, Adolph HG (1979) Propell Explos Pyrotech 4:30–34
8. Engelke R, Earl WL, Rohlfing CM (1986) J Chem Phys 84:142
9. Politzer P, Seminario JM, Zacarías AG (1996) Mol Phys 89:1511–1520
10. Murray JS, Lane P, Göbel M, Klapötke TM, Politzer P (2009) J Chem Phys 130:104304
11. Schödel H, Dienelt R, Bock H (1994) Acta Cryst C50:1790–1792
12. Urbanski T (1984) Chemistry and technology of explosives, vol 4. Pergamon, Oxford, UK
13. Andrew LW, Hammick DL (1934) J Chem Soc 244
14. Novikov SS, Slovetskii VI, Tartakovskii VA, Shevelev SA, Fainzil'berg AA (1962) Dokl Akad Nauk SSSR 146:104
15. Novikov SS, Slovetskii VI, Tartakovskii VA, Shevelev SA, Fainzil'berg AA (1963) Chem Abstr 58:3289
16. Meyer R, Köhler J, Hornburg A (2007) Explosives, 6th edn. Wiley-VCH, Weinheim, Germany
17. Fukui K (1981) Acc Chem Res 14:363–368
18. Gonzalez C, Schlegel HB (1990) J Phys Chem 94:5523–5527
19. Toro-Labbé A (1999) J Phys Chem A 103:4398–4403
20. Martínez J, Toro-Labbé A (2004) Chem Phys Lett 392:132–140
21. Toro-Labbé A, Gutiérrez-Oliva S, Concha MC, Murray JS, Politzer P (2004) J Chem Phys 121:4570–4576
22. Herrera B, Toro-Labbé A (2004) J Chem Phys 121:7096–7102
23. Politzer P, Toro-Labbé A, Gutiérrez-Oliva S, Herrera B, Jaque P, Concha MC, Murray JS (2005) J Chem Sci 117:467–472
24. Gutiérrez-Oliva S, Herrera B, Toro-Labbé A, Chermette H (2005) J Phys Chem A 109:1748–1751
25. Politzer P, Burda JV, Concha MC, Lane P, Murray JS (2006) J Phys Chem A 110:756–761
26. Rincón E, Jaque P, Toro-Labbé A (2006) J Phys Chem A 110:9478–9485
27. Politzer P, Murray JS, Lane P, Toro-Labbé A (2007) Int J Quantum Chem 107:2153–2157
28. Burda JV, Toro-Labbé A, Gutiérrez-Oliva S, Murray JS, Politzer P (2007) J Phys Chem A 111:2455–2458
29. Toro-Labbé A, Gutiérrez-Oliva S, Murray JS, Politzer P (2007) Mol Phys 105:2619–2625
30. Herrera B, Toro-Labbé A (2007) J Phys Chem A 111:5921–5926
31. Toro-Labbé A, Gutiérrez-Oliva S, Politzer P, Murray JS (2008) In: Chattaraj P (ed) Theory of chemical reactivity, chap 21. Taylor-Francis, Boca Raton, FL
32. Labet V, Morell C, Grand A, Toro-Labbé A (2008) J Phys Chem A 112:11487–11494
33. Echegaray E, Toro-Labbé A (2008) J Phys Chem A 112:11801–11807
34. Jaque P, Toro-Labbé A, Politzer P, Geerlings P (2008) Chem Phys Lett 456:135–140
35. Politzer P, Murray JS (2008) Collect Czech Chem Commun 73:822–830
36. Murray JS, Toro-Labbé A, Clark T, Politzer P (2009) J Mol Model 15:701–706
37. Toro-Labbé A, Gutiérrez-Oliva S, Murray JS, Politzer P (2009) J Mol Model 15:707–710
38. Jaque P, Toro-Labbé A, Geerlings P, De Proft F (2009) J Phys Chem A 113:332–344
39. Burda JV, Murray JS, Toro-Labbé A, Gutiérrez-Oliva S, Politzer P (2009) J Phys Chem A 113:6500–6505
40. Polanyi JC, Zewail AH (1995) Acc Chem Res 28:119–132
41. Zewail AH (2000) J Phys Chem A 104:5660–5694
42. Murray JS, Concha MC, Politzer P (2009) Mol Phys 107:89–97
43. Caminati W, Wilson EB (1980) J Mol Spectrosc 81:507–510
44. Levchenkov DV, Kharitonkov AB, Shlyapochnikov VA (2001) Russ Chem Bull 50:385–389
45. Göbel M, Klapötke TM (2007) Acta Cryst C63:o562–o564
46. Göbel M, Klapötke TM (2009) Adv Funct Mater 19:347–365
47. Göbel M, Tchitchanov BH, Murray JS, Politzer P, Klapötke TM (2009) Nature Chem 1:229–235
48. Lammertsma K, Bharatam PV (2000) J Org Chem 65:4662–4670
49. Harris NJ, Lammertsma K (1996) J Am Chem Soc 118:8048–8055
50. Bondi A (1964) J Phys Chem 68:441–451